Three-Body Correlations in Nuclear Matter*

B. D. Day
Argonne National Laboratory, Argonne, Illinois 60439,† and Niels Bohr Institute, Copenhagen, Denmark

and

F. Coester and A. Goodman
Argonne National Laboratory, Argonne, Illinois 60439

(Received 10 July 1972)

The possibility of computing the three-body correlation energy in nuclear matter by direct solution of integral equations in momentum space is studied. An important feature of the procedure is that the off-energy-shell reaction matrix, which comes from an arbitrary two-body potential, is approximated by a sum of separable terms. Detailed numerical calculations are made for an S-wave force consisting of the Reid $^1S_0$ potential acting in both singlet and triplet states. The main results are as follows: (1) The Reid $^1S_0$ reaction matrix can be accurately represented by two or three separable terms for all relative momenta k in the region $0 < k < 8$ fm^{-1}. This is the relevant region for the calculations. (2) Integrals over momenta can be adequately approximated by finite sums over only 6 or 8 Gauss points. (3) Many three-body states can be adequately treated in lowest order and therefore do not appear in the integral equations. On the basis of these results, it is estimated that a calculation using the full nuclear force would require the solution of systems of 100–200 linear equations. Solving such systems is perfectly feasible with present-day computers. The three-body correlation energy has been calculated at three different densities for the assumed two-body force.

I. INTRODUCTION

Recent calculations[1] of the binding energy of nuclear matter give 13.7 MeV per particle, about 2 MeV short of the value deduced from the semi-empirical mass formula.[2] However, the theoretical result contains an uncertainty of about 2 MeV due to the computational difficulty in evaluating the higher-order terms in Brueckner theory. Since the calculational uncertainty is comparable to the discrepancy between the empirical and theoretical results, improved calculations are clearly needed. In the present work, we consider the possibility of making more accurate calculations of the three-body correlation energy in nuclear matter.

The work of Rajaraman[3] and Bethe[4] showed that a correct treatment of three-body correlations requires summing the three-body cluster diagrams to all orders. This is equivalent to solving a three-body integral equation. A simple and practical approximation method which makes use of coordinate-space wave functions was given by Bethe[4] and was improved by Day,[5] Kirson,[6] Bethe,[7] and Dahlblom.[8] It has also been discussed by Moszkowski,[9] and simple tests[10] have been made by Easlea and by Petschek. A different type of calculation, using a separable S-wave force, has been made by Bhakar and McCarthy.[11] However, the only published calculation using the full nuclear force is that of Dahlblom.[8]

Dahlblom treated both the Reid[12] hard-core and Yukawa-core potentials, using the coordinate-space method mentioned above. This method involves a number of different approximations, all of which are well understood on physical grounds. But it is very hard to make a quantitative estimate of the combined error produced by the various approximations. An error as large as 1–2 MeV does not seem impossible. In any case, it would clearly be valuable to check Dahlblom's result in a completely independent calculation.

The coordinate-space method gives very good physical understanding, but it is not the first step in a systematic approximation scheme. To obtain better numerical accuracy, it seems better to work in momentum space. Numerical techniques such as Gaussian integration are more efficient in momentum space because the two-body wave function is smoother in momentum space than in coordinate space. Therefore, in the present work the possibility of doing accurate calculations in momentum space is studied.

Depp[13] has given a detailed and complete derivation of a system of three-body momentum-space equations for nuclear matter. He obtains a system of coupled integral equations in two continuous variables for the three-body reaction matrix. He

has also done some preliminary numerical calculations and his work clearly shows that, for a realistic nuclear force, the computational problem is a big one.

Therefore, it seems sensible to gain some numerical experience on a smaller problem before attempting a calculation using the full nuclear force. We have therefore studied the problem with a pure S-state force that consists of the Reid $^1S_0$ potential acting in both singlet and triplet states. The problem is then small enough that we can study in detail such questions as, how many mesh points are needed in momentum space, where can integrals in momentum space be safely cut off, etc.

Ordinarily such numerical details are of little interest; but the present computational problem is so large that any results that help to define its size are valuable, and our results do this. They enable us to make a rough estimate of the size of the full problem involving a realistic two-body force. The main question is: After integrals have been approximated by finite sums, how many simultaneous linear equations must be solved? Our results make it probable that this number is between 100 and 200. This is a large number of linear equations, but it is well within the capabilities of existing computers.

We have also made detailed calculations of the three-body correlation energy at three different densities for our assumed S-wave force. However, these results seem to offer no adequate basis for an estimate of how much energy the full Reid potential would give.

Our equations are set up somewhat differently from Depp's. For example, we differ from him in using a separable approximation to the two-body reaction matrix. Therefore, in Sec. II we give a derivation of the equations we have used. In Sec. III, these equations are reduced to a form suitable for computation, and numerical results are presented. These results are discussed in Sec. IV.

II. THREE-BODY EQUATIONS

Exact equations for the binding energy of nuclear matter have been derived previously.[14] The energy involves a two-body operator W_2 that is determined by a fairly complicated set of nonlinear equations.[15] An iterative solution adapted to the properties of hard potentials gives successive approximations to W_2 in the form

$$W_2 = \sum_{n=2}^{\infty} W_2^{(n)}, \tag{2.1}$$

where each $W_2^{(n)}$ is obtained as the solution of a linear integral equation. $W_2^{(2)}$ is given by the reaction matrix. The equation for $W_2^{(3)}$ is the subject of the present paper. Formal iteration of the integral equation for $W_2^{(3)}$ generates the series of three-body-cluster diagrams for nuclear matter. Since this series is expected to diverge,[3,4] it is the integral equation that is more fundamental and that should be used in numerical calculations.

For any two-momenta $\vec{p}_1$ and $\vec{p}_2$ below the Fermi level k_F, the total momentum $\vec{P}_0$ and the relative momentum $\vec{k}_0$ are

$$\vec{P}_0 = \vec{p}_1 + \vec{p}_2, \tag{2.2}$$

$$\vec{k}_0 = \tfrac{1}{2}(\vec{p}_1 - \vec{p}_2). \tag{2.3}$$

The energy per particle, expressed in terms of the momentum-space kernel of W_2, is[16]

$$\mathcal{E} = 0.3k_F^2 + \tfrac{1}{2}(2\pi)^{-3}\rho^{-1}\int d^3P_0' \int d^3P_0 \int d^3k_0 Q_h(\vec{P}_0, \vec{k}_0)(\vec{k}_0, \vec{P}_0' | W_2 | \vec{P}_0, \vec{k}_0), \tag{2.4}$$

where the particle density ρ is given by

$$\rho = 2k_F^3/3\pi^2. \tag{2.5}$$

If the momenta are measured in fm^{-1}, then conversion of the energy to MeV requires multiplication by 41.47 MeV fm^2. The double integral over $\vec{P}_0'$ and $\vec{P}_0$ is necessary since the kernel of W_2 contains a δ function $\delta(\vec{P}_0' - \vec{P}_0)$. The operator Q_h is the projection operator that requires both $\vec{p}_1$ and $\vec{p}_2$ to be below the Fermi level. Spin and isospin variables are implied. They are suppressed at this time for the sake of brevity, but will appear explicitly at the appropriate later stage.

Self-consistent single-particle energies $\epsilon(p)$ for $p < k_F$ are given by

$$\delta(\vec{p}' - \vec{p})\epsilon(p) = \delta(\vec{p}' - \vec{p})\tfrac{1}{2}p^2 + \int d^3p''(\vec{p}', \vec{p}'' | W_2 | \vec{p}'', \vec{p}). \tag{2.6}$$

The leading term in W_2 is

$$(\vec{k}, \vec{P} | W_2^{(2)} | \vec{P}_0, \vec{k}_0) = \delta(\vec{P} - \vec{P}_0)(\vec{k} | G(\omega, \vec{P}) | \vec{k}_0), \tag{2.7}$$

where

$$\omega = \epsilon(p_1) + \epsilon(p_2) \tag{2.8}$$

and the reaction matrix G is defined by the two-body operator equation

$$G = \{1 + V(Q/e)\}^{-1} V. \tag{2.9}$$

The projection operator $Q(\vec{P}, \vec{k})$ requires both particles to be above the Fermi level. The operator e is defined by

$$e\psi(\vec{k}_1, \vec{k}_2) = [\epsilon(k_1) + \epsilon(k_2) - \omega]\psi(\vec{k}_1, \vec{k}_2), \tag{2.10}$$

where the single-particle energy $\epsilon(k)$ for $k > k_F$ is the kinetic energy

$$\epsilon(k) = \tfrac{1}{2}k^2. \tag{2.11}$$

We have thus

$$e\psi(\vec{P}, \vec{k}) = (\tfrac{1}{4}P^2 + k^2 - \omega)\psi(\vec{P}, \vec{k}). \tag{2.12}$$

Two-body wave functions are antisymmetric, and the normalization integral is

$$\|\psi\|^2 = \tfrac{1}{2}\int d^3k_1 \int d^3k_2 |\psi(\vec{k}_1, \vec{k}_2)|^2. \tag{2.13}$$

In order to discuss the equations for $W_2^{(3)}$, it is convenient to introduce three-body wave functions $\psi(\vec{k}_1, \vec{k}_2; \vec{k}_3)$ which are antisymmetric only in the first two particles. They satisfy the relations

$$\psi(\vec{k}_1, \vec{k}_2; \vec{k}_3) = -\psi(\vec{k}_2, \vec{k}_1; \vec{k}_3), \tag{2.14}$$

$$\|\psi\|^2 = \tfrac{1}{2}\int d^3k_1 \int d^3k_2 \int d^3k_3 |\psi(\vec{k}_1, \vec{k}_2; \vec{k}_3)|^2. \tag{2.15}$$

We define the permutation operator X by

$$X\psi(\vec{k}_1, \vec{k}_2; \vec{k}_3) = \psi(\vec{k}_2, \vec{k}_3; \vec{k}_1) + \psi(\vec{k}_3, \vec{k}_1; \vec{k}_2). \tag{2.16}$$

Note that $\frac{1}{3}(1 + X)$ is the projection operator that projects out the fully antisymmetric component.

Instead of the single-particle momenta $\vec{k}_1, \vec{k}_2, \vec{k}_3$, we may use relative and total momenta when convenient. These are related by

$$\begin{aligned} \vec{k} &= \tfrac{1}{2}(\vec{k}_1 - \vec{k}_2), \\ \vec{\mathfrak{K}} &= \vec{k}_1 + \vec{k}_2 + \vec{k}_3 = \vec{P} + \vec{k}_3, \\ \vec{P} &= \vec{k}_1 + \vec{k}_2 = \tfrac{2}{3}\vec{\mathfrak{K}} + \vec{K}, \\ \vec{K} &= \tfrac{1}{3}\vec{P} - \tfrac{2}{3}\vec{k}_3. \end{aligned} \tag{2.17}$$

The kernel of $W_2^{(3)}$ has the form[16]

$$(\vec{k}_0', \vec{P}_0' | W_2^{(3)} | \vec{P}_0, \vec{k}_0) = \int_{|\vec{p}_3| < k_F} d^3p_3 (\vec{k}_0', \vec{P}_0'; \vec{p}_3 | \tilde{G}(\omega)(Q/e)X W_3 | \vec{p}_3; \vec{P}_0, \vec{k}_0), \tag{2.18}$$

where Q is the projection operator that requires the first two particles to be above the Fermi level and

$$\omega = \epsilon(p_1) + \epsilon(p_2) + \epsilon(p_3). \tag{2.19}$$

The single-particle momenta $\vec{p}_1$ and $\vec{p}_2$ correspond to $\vec{P}_0$ and $\vec{k}_0$. The three-body energy denominator e is given by

$$e\psi(\vec{k}_1, \vec{k}_2; \vec{k}_3) = [\epsilon(k_1) + \epsilon(k_2) + \epsilon(k_3) - \omega]\psi(\vec{k}_1, \vec{k}_2; \vec{k}_3). \tag{2.20}$$

The three-body operator $\tilde{G}(\omega)$ is related to the reaction matrix by

$$(\vec{k}', \vec{P}'; \vec{k}_3' | \tilde{G}(\omega) | \vec{k}_3; \vec{P}, \vec{k}) = \delta(\vec{P}' - \vec{P})\delta(\vec{k}_3' - \vec{k}_3)(\vec{k}' | G[\omega - \epsilon(k_3)] | \vec{k}). \tag{2.21}$$

The operator W_3 is the solution of the equation[17]

$$W_3|\vec{p}_3,\vec{p}_2,\vec{p}_1\rangle=\{\tilde{G}(\omega)X(Q/e)\tilde{G}(\omega)(1+X)-\tilde{G}(\omega)X(Q/e)W_3\}|\vec{p}_3,\vec{p}_2,\vec{p}_1\rangle\,. \tag{2.22}$$

It will be convenient in the future to label the symbol $\tilde{G}$ to indicate whether the spectator momentum k_3 is above or below the Fermi level. We use $\tilde{G}_a$ and $\tilde{G}_b$, respectively.

Because of the translational invariance, all operators commute with the total momentum $\vec{\mathfrak{K}}$. It is therefore possible and convenient to redefine all three-body operators as operators on functions $\psi(\vec{k},\vec{K})$ depending on the total momentum as a parameter. We do this without introducing new symbols for the operators.

Putting Eq. (2.18) into Eq. (2.4) and using Eq. (2.22), we find that the three-body correlation energy $\mathcal{E}_3$ can be written in the form

$$\mathcal{E}_3=\tfrac{1}{2}(2\pi)^{-3}\rho^{-1}\int d^3\mathfrak{K}_0\int d^3K_0\int d^3k_0 Q_h(\vec{\mathfrak{K}}_0,\vec{K}_0,\vec{k}_0)(\vec{k}_0,\vec{K}_0|F_0^{\dagger}F(1+X)|\vec{K}_0,\vec{k}_0)\,, \tag{2.23}$$

where by definition

$$F_0|\vec{K}_0,\vec{k}_0\rangle=X(Q/e)\tilde{G}_b(\omega)|\vec{K}_0,\vec{k}_0\rangle \tag{2.24}$$

and F satisfies the equation

$$F=\tilde{G}_a[F_0-BF] \tag{2.25}$$

with

$$B\equiv XQ/e\,. \tag{2.26}$$

The projection operator Q_h requires all three particles to be below the Fermi level.

Equations (2.23)–(2.26) can also be obtained by a formal summation of the three-body-cluster diagrams. We now briefly indicate the correspondence between the formulas and the diagrams. We follow Depp[13] and use Hugenholtz[18] diagrams. Then in each order of perturbation theory there are just two three-body cluster diagrams. Diagrams such as those of Figs. 1(a) and 1(c), in which two hole lines proceed undisturbed from the highest to the lowest vertex, are called direct diagrams. All others, such as 1(b) and 1(d), are called exchange diagrams.

To see the connection between the formulas and the diagrams, consider first the direct third-order diagram 1(a). Using the definition (2.21) of $\tilde{G}$, we can write its contribution to $\mathcal{E}$ in a form similar to Eq. (2.23). The result is

$$\mathcal{E}_3=\tfrac{1}{2}(2\pi)^{-3}\rho^{-1}\prod_i^3\int_{|p_i|<k_F}d^3p_i(\vec{p}_1,\vec{p}_2;\vec{p}_3|M^{(3)}|\vec{p}_3;\vec{p}_2,\vec{p}_1)\,, \tag{2.27}$$

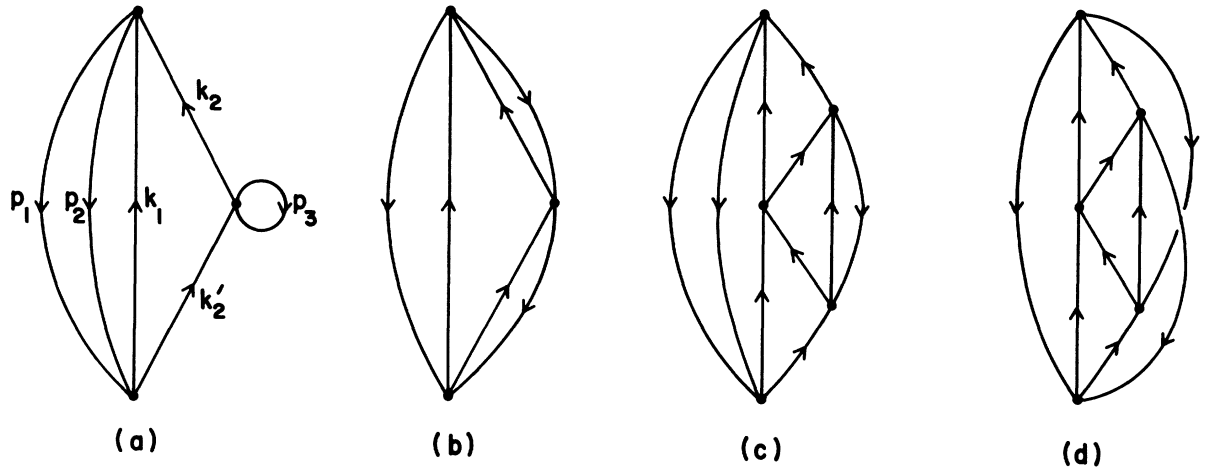

FIG. 1. Three-body-cluster diagrams in the Hugenholtz representation. (a) Direct third-order diagram. (b) Exchange third-order diagram. (c) Direct fifth-order diagram. (d) Exchange fifth-order diagram.

where

$$(\vec{p}_1,\vec{p}_2;\vec{p}_3|M^{(3)}|\vec{p}_3;\vec{p}_2,\vec{p}_1)=\int\prod_i^3 d\vec{k}_i d\vec{k}_i'(\vec{p}_1,\vec{p}_2;\vec{p}_3|\tilde{G}_b(\omega)(Q/e)|\vec{k}_3;\vec{k}_2,\vec{k}_1)$$
$$\times(\vec{k}_2,\vec{k}_3;\vec{k}_1|\tilde{G}_a(\omega)|\vec{k}_3';\vec{k}_2',\vec{k}_1')(\vec{k}_2',\vec{k}_3';\vec{k}_1'|(Q/e)\tilde{G}_b(\omega)|\vec{p}_3;\vec{p}_2,\vec{p}_1)\,. \tag{2.28}$$

With our normalization, we have

$$\langle\vec{k}_1,\vec{k}_2;\vec{k}_3|\vec{k}_3';\vec{k}_2',\vec{k}_1'\rangle=\delta(\vec{k}_3-\vec{k}_3')[\delta(\vec{k}_1-\vec{k}_1')\delta(\vec{k}_2-\vec{k}_2')-\delta(\vec{k}_1-\vec{k}_2')\delta(\vec{k}_2-\vec{k}_1')]\,. \tag{2.29}$$

This can be used with (2.16) to obtain

$$X=\int\prod_i d\vec{k}_i|\vec{k}_3;\vec{k}_2,\vec{k}_1\rangle\langle\vec{k}_2,\vec{k}_3;\vec{k}_1|\,. \tag{2.30}$$

Putting this into Eq. (2.28) gives

$$M^{(3)}=F_0^{\dagger}F^{(1)}\,, \tag{2.31}$$

where $F^{(1)}\equiv\tilde{G}_aF_0$ is the first-order term in the integral equation (2.25) for F.

Thus the third-order direct diagram represents the expression (2.23), except that F is replaced by $F^{(1)}$, and only the "1" is used from "$1+X$." The same statement holds for the direct diagram of order $n+2$, except that F is now replaced by its nth iterate $F^{(n)}=(-\tilde{G}_aB)^{n-1}\tilde{G}_aF_0$. Therefore, iteration of the integral equation (2.25) generates order by order all the direct diagrams. The exchange diagrams are generated in exactly the same way, except that in Eq. (2.23) the "X" is used from "$1+X$."

Our task is to solve Eq. (2.25) for fixed $\vec{\mathcal{K}}_0$, $\vec{K}_0$, and $\vec{k}_0$, evaluate the integrand in Eq. (2.23), and sum over $\vec{\mathcal{K}}_0$, $\vec{K}_0$, and $\vec{k}_0$. Two main features are involved in reducing Eq. (2.25) to a manageable form for numerical computation: The separable approximation for the reaction matrix and the exploitation of rotational symmetry. The latter involves the use of the partial-wave representation, certain angle averages, and the assumption of an S-wave force. We proceed to discuss these steps in turn.

The separable approximation will be applied to $\tilde{G}_a$ but not to $\tilde{G}_b$. We have

$$(\vec{k}',\vec{K}'|\tilde{G}_a|\vec{K},\vec{k})=\delta(\vec{K}'-\vec{K})(\vec{k}'|G(\vec{K})|\vec{k}) \tag{2.32}$$

since Q is a function of $\vec{P}=\frac{2}{3}\vec{\mathcal{K}}_0+\vec{K}$ and

$$e=\tfrac{1}{6}\mathcal{K}_0^2+\tfrac{3}{4}K^2+k^2-\omega\,. \tag{2.33}$$

It is reasonable to expect that very high values of k and k' do not contribute significantly to the integrals. We assume that

$$(\vec{k}|G|\vec{k}')=0$$

unless k and k' are both less than a finite upper limit $k_{\max}$. We have tested this by varying the cutoff $k_{\max}$.

Since this truncated kernel represents a compact operator, it may be approximated by a kernel of finite rank. Since low k are expected to be more important than high k, we prefer to approximate the weighted kernel wG_aw, where $w(\vec{k},\vec{K})$ is a positive weight function which decreases with increasing k. We have then

$$w(\vec{k},\vec{K})(\vec{k}|G(\vec{K})|\vec{k}')w(\vec{k}',\vec{K})\approx\sum_{i,j}\lambda_{ij}(\vec{K})s_i(\vec{k},\vec{K})s_j^*(\vec{k}',\vec{K})\,, \tag{2.34}$$

where λ_{ij} is a finite Hermitian matrix and the functions $s_i(\vec{k})$ are conveniently chosen interpolating functions. Let $u_{i\beta}$ and λ_β be the eigenvectors and eigenvalues of the matrix λ_{ij}. Then it follows from Eq. (2.34) that

$$(\vec{k}|G|\vec{k}')\approx\sum_\beta g_\beta(\vec{k},\vec{K})\lambda_\beta(\vec{K})g_\beta(k',\vec{K})^*\,, \tag{2.35}$$

where

$$g_\beta(\vec{k},\vec{K})=\sum_i u_{i\beta}s_i(\vec{k},\vec{K})/w(\vec{k},\vec{K})\,. \tag{2.36}$$

The values of β with the largest $|\lambda_\beta|$ contribute the most to this sum, while small eigenvalues contribute very little. This is the basis for the important approximation in which we restrict the sum over β to a few terms only. In actual calculations, the dimension of the matrix λ_{ij} is 35 while the number of β's re-

tained varies between 2 and 5. It follows from Eqs. (2.25), (2.35), and (2.36) that

$$(\vec{k},\vec{K}\,|\,F\,|\,\vec{K}_0,\vec{k}_0)\approx\sum_\beta F(\beta,\vec{K})g_\beta(\vec{k},\vec{K})\,. \tag{2.37}$$

The functions $F(\beta,\vec{K})$ are then the solution of the equation

$$F(\beta,\vec{K})=\lambda_\beta(\vec{K})F_0(\beta,\vec{K})-\lambda_\beta(\vec{K})\sum_{\beta'}\int d^3K'(\beta,\vec{K}\,|\,B\,|\,\vec{K}',\beta')F(\beta',\vec{K}')\,, \tag{2.38}$$

where

$$F_0(\beta,\vec{K})=\frac{1}{2}\int d^3k\,g^*_\beta(\vec{k},\vec{K})(\vec{k},\vec{K}\,|\,X(Q/e)\tilde{G}_b\,|\,\vec{K}_0,\vec{k}_0) \tag{2.39}$$

and

$$(\beta,\vec{K}\,|\,B\,|\vec{K}',\beta')=\frac{1}{4}\int d^3k\int d^3k'\,g^*_\beta(\vec{k},\vec{K})(\vec{k},\vec{K}\,|\,X(Q/e)\,|\,\vec{K}',\vec{k}')g_{\beta'}(\vec{k}',\vec{K}')\,. \tag{2.40}$$

It follows from these definitions that

$$(\vec{k}_0,\vec{K}_0\,|\,F_0^\dagger F\,|\,\vec{K}_0,\vec{k}_0)\approx\sum_\beta\int d^3K\,F_0^*(\beta,\vec{K})F(\beta,\vec{K})\,. \tag{2.41}$$

The rotational symmetry of our problem is enhanced by assuming pure S-wave potentials and by using angle averages. For the two-body projection operator Q, we use the angle average $\overline{Q}(P,k)$, which is known to give good results for the leading term in the potential energy.[19] We also average out any dependence on the direction of the total momentum $\vec{\mathfrak{K}}_0$. The direction of $\vec{\mathfrak{K}}_0$ enters g_β and λ_β only via

$$P^2=|\tfrac{2}{3}\vec{\mathfrak{K}}_0+\vec{K}|^2\,. \tag{2.42}$$

We replace P^2 by its angle average

$$\overline{P}^2=\tfrac{4}{9}\mathfrak{K}_0^2+K^2\,. \tag{2.43}$$

It follows that λ_β and g_β depend only on the magnitudes of $\vec{k}$ and $\vec{K}$.

The transformation to the partial-wave representation is given by

$$(\vec{K},\vec{k}\,|\,k,l,m,K,L,M)=\frac{\delta(|\vec{K}|-K)}{K}\,\frac{\delta(|\vec{k}|-k)}{k}\,Y_{LM}(\hat{K})Y_{lm}(\hat{k})\,. \tag{2.44}$$

At this point we must explicitly introduce the spin and isospin variables which were suppressed so far. Let S be the total spin of particles 1 and 2 while $\mathcal{S}$ is the total spin of all three particles. The isospin is coupled in the same fashion. Thus the representation used for our numerical calculations has the quantum numbers $\vec{\mathfrak{K}},K,L,M,k,l,m,\mathcal{S},\mathcal{S}_z,\mathcal{T},\mathcal{T}_z,S,T$. When the full nuclear force is taken into account, further coupling of angular momenta is desirable.[13,20] But this is unnecessary for the present purpose. Restriction to S-wave potentials and angle averaging implies that $l=m=0$ throughout, and all operators commute with $\vec{L}$, $\vec{\mathcal{S}}$, and $\vec{\mathcal{T}}$. The kernels are therefore independent of M, $\mathcal{S}_z$, and $\mathcal{T}_z$, and these quantum numbers will be dropped in the following. Because of the exclusion principle and $l=0$, the pair of variables (S,T) is restricted to $(0,1)$ and $(1,0)$. Since

$$Y_{00}^{\,2}=(4\pi)^{-1} \tag{2.45}$$

and

$$\sum_M Y_{LM}(\hat{K})Y^*_{LM}(\hat{K})=(2L+1)/4\pi\,, \tag{2.46}$$

the energy $\mathcal{E}_3$ is

$$\mathcal{E}_3=\tfrac{1}{2}(2\pi)^{-3}(4\pi)^{-2}\rho^{-1}\int d^3\mathfrak{K}_0\int d^3K_0\int d^3k_0\,Q_h(\vec{\mathfrak{K}}_0,\vec{K}_0,\vec{k}_0)\sum_{L\mathcal{S}\mathcal{T}}(2L+1)(2\mathcal{S}+1)(2\mathcal{T}+1)$$
$$\times\sum_{S_0T_0}(k_0,K_0,S_0,T_0\,|\,F_0^\dagger F(1+X)\,|\,T_0,S_0,K_0,k_0)K_0^{-2}k_0^{-2}\,. \tag{2.47}$$

The conserved quantum numbers $\vec{\mathfrak{K}}_0$, L, $\mathcal{S}$, $\mathcal{T}$ are implied.

The kernel of the operator X depends on the conserved quantum numbers L, $\mathcal{S}$, $\mathcal{T}$ but not on $\vec{\mathfrak{K}}_0$. It has

been evaluated by Depp,[13] and by Balian and Brézin.[21] We have

$$(k', K', S', T'|X(L, \mathcal{S}, \mathcal{T})|T, S, K, k) = 4\theta(1-|z|)(k', K'|f(L)|K, k) \times \delta(\tfrac{3}{4}K^2 + k^2 - \tfrac{3}{4}K'^2 - k'^2)(S', T'|\mathcal{R}(\mathcal{S}, \mathcal{T}|T, S), \tag{2.48}$$

$$(k', K'|f(L)|K, k) = P_L(z), \tag{2.49}$$

where θ is the unit step function, P_L is the Legendre polynomial, and

$$z = [\tfrac{1}{2}(k^2 + k'^2) - \tfrac{5}{8}(K^2 + K'^2)]/(KK'). \tag{2.50}$$

The expression $\frac{3}{4}K^2 + k^2$ is the kinetic energy of the relative motion of the three particles and is therefore invariant under permutations. The δ function expresses this invariance. The spin-isospin matrix $\mathcal{R}(\mathcal{S}, \mathcal{T})$ has the values

$$\mathcal{R}(\tfrac{1}{2}, \tfrac{3}{2}) = \mathcal{R}(\tfrac{3}{2}, \tfrac{1}{2}) = -1, \tag{2.51}$$

$$\mathcal{R}(\tfrac{1}{2}, \tfrac{1}{2}) = \frac{1}{2}\begin{pmatrix} 1 & -3 \\ -3 & 1 \end{pmatrix}. \tag{2.52}$$

When $\mathcal{S} \neq \mathcal{T}$, only one value of (S, T) is allowed.

The final form for F_0 is then

$$F_0(\beta, K, S, T) = \frac{1}{4}\int dk \int dk' g_\beta(k, K)(k, K, S, T|X|T_0, S_0, K_0, k')[\bar{Q}(K_0, k')/e_2(k')](k'|G|k_0), \tag{2.53}$$

where

$$e_2(k') = k'^2 + \tfrac{1}{4}\bar{P}^2 - \epsilon(p_1) - \epsilon(p_2) \approx k'^2 + \tfrac{1}{9}\mathcal{K}_0^2 + \tfrac{1}{4}K_0^2 - \tfrac{2}{3}\omega. \tag{2.54}$$

Similarly, for B we have

$$(\beta, K, S, T|B|T', S', K', \beta') = \frac{1}{4}\int dk \int dk' g_\beta(k, K) \times (k, K, S, T|X|T', S', K', k')[\bar{Q}(K', k')/e_3(k', K')]g_{\beta'}(k', K'), \tag{2.55}$$

where

$$e_3(k', K') = \tfrac{1}{6}\mathcal{K}_0^2 + \tfrac{3}{4}K'^2 + k'^2 - \omega. \tag{2.56}$$

III. NUMERICAL CALCULATIONS

A. Formulas Used for Computation

In this section we write out the formulas that were actually used for numerical calculation. Consider first formulas (2.53) and (2.55) for the inhomogeneous term F_0 and the kernel B of the integral equation. In each of these, we insert Eq. (2.48) for the matrix element of X and use the δ function to carry out the integral over k. The resulting equations are

$$F_0(\beta, K, S, T) = \tfrac{1}{2}(S, T|\mathcal{R}(\mathcal{S}, \mathcal{T})|T_0, S_0)\int_{L(K, K_0)}^{K+\frac{1}{2}K_0}(dk'/k)g_{\beta S T}(k, K) \times (k, K|f(L)|K_0, k')[\bar{Q}(K_0, k')/e_2(k')](k'|G(K_0, S_0, T_0)|k_0), \tag{3.1}$$

$$(\beta, K, S, T|B|T', S', K', \beta') = \tfrac{1}{2}(S, T|\mathcal{R}(\mathcal{S}, \mathcal{T})|T', S')\int_{L(K, K')}^{K+\frac{1}{2}K'}(dk'/k)g_{\beta S T}(k, K) \times (k, K|f(L)|K', k')[\bar{Q}(K', k')/e_3(k', K')]g_{\beta' S' T'}(k', K'), \tag{3.2}$$

where

$$L(K, K') = \max\left\{\begin{matrix} |K - \tfrac{1}{2}K'| \\ (k_F^2 - \tfrac{1}{9}\mathcal{K}_0^2 - \tfrac{1}{4}K'^2)^{1/2} \end{matrix}\right\}, \tag{3.3}$$

and it is understood that any integral whose lower limit exceeds its upper limit is to be put equal to zero. The matrix element of $f(L)$ in Eq. (3.1) shows that the momenta (k, K) give the same kinetic energy as (k', K_0). This determines the value of k in Eq. (3.1), and a similar remark applies to Eq. (3.2).

The limits of integration in these formulas require some discussion. The definition of the matrix element $f(L)$ in Eq. (3.1) by Eqs. (2.49) and (2.50) implies the requirement that $|z|<1$. This implies in Eq. (3.1) that $|K-\frac{1}{2}K_0|<k'<K+\frac{1}{2}K_0$. Another condition on k' is that $\overline{Q}(K_0, k')$ be nonzero, i.e., that $k'^2+\frac{1}{4}\overline{P}^2 > k_F^2$, where $\overline{P}$ is defined by Eq. (2.43). This gives a second lower limit on k', and Eq. (3.3) is simply the statement that k' must be greater than each of these lower limits. A similar discussion holds for the limits on k' in Eq. (3.2).

An additional restriction on the upper limits of integration in Eqs. (3.1) and (3.2) comes from the requirement that k and k' both be less than the cutoff value $k_{\max}$ for relative momenta. In numerical work we have always taken $k_{\max}$ equal to the cutoff value $K_{\max}$ used in Eq. (3.4).

From Eq. (2.38) it follows that the integral equation for F is

$$[\lambda_{\beta S T}(K)]^{-1}F(\beta, K, S, T) = F_0(\beta, K, S, T) - \sum_{\beta' S' T'} \int dK' (\beta, K, S, T|B|T', S', K', \beta')F(\beta', K', S', T'), \tag{3.4}$$

where $K_{\min} \leq K' \leq K_{\max}$. The cutoff momentum $K_{\max}$ is to be taken large enough so that the error in the integral is negligible. What value should be used for $K_{\min}$? The kernel B given by Eq. (3.2) has nonzero matrix elements for all $K>0$. However, Eqs. (2.39) and (2.40) imply that the solution F is nonzero only in momentum-space regions in which $|\vec{k}_3|>k_F$. From Eq. (2.17) we find $\vec{k}_3=\frac{1}{3}\vec{\mathcal{K}}_0-\vec{K}$, so that we must require

$$k_3^2 = \tfrac{1}{9}\mathcal{K}_0^2 + K^2 - \tfrac{2}{3}\mathcal{K}_0 K\cos\theta > k_F^2, \tag{3.5}$$

where θ is the angle between $\vec{\mathcal{K}}_0$ and $\vec{K}$. Since $|\cos\theta|<1$, Eq. (3.5) shows that K must be greater than some lower limit in order that the solution F be nonzero.

A nonzero lower limit on K also arises from the fact that the allowed region of momentum space for F is exactly the same as for $\tilde{G}_a F_0$. The allowed region consists of all points $\{\vec{k}_1, \vec{k}_2, \vec{k}_3\}$ with total momentum equal to $\vec{\mathcal{K}}_0$ and $|\vec{k}_3|>k_F$. Starting with momenta $\{\vec{p}_1, \vec{p}_2, \vec{p}_3\}$ in the Fermi sea, one can reach any point in the allowed region via two two-body interactions. Since $\tilde{G}_a F_0$ involves two two-body interactions, it is nonzero in the same region as F. But $\tilde{G}_a F_0$ is represented by Eq. (3.1), which is nonzero only when $K+\frac{1}{2}K_0 > L(K, K_0)$, i.e., only when

$$K > (k_F^2 - \tfrac{1}{9}\mathcal{K}_0^2 - \tfrac{1}{4}K_0^2)^{1/2} - \tfrac{1}{2}K_0. \tag{3.6}$$

Thus F is nonzero only when K satisfies Eq. (3.6).

Both of these lower limits on K have been lost in our equations because of our use of the angle-averaged Pauli operator $\overline{Q}$. But we reimpose them by our choice of $K_{\min}$. Condition (3.6) is most restrictive when $K_0=0$, and this determines the value of $K_{\min}$ that we actually use, namely,

$$K_{\min} = (k_F^2 - \tfrac{1}{9}\mathcal{K}_0^2)^{1/2}. \tag{3.7}$$

The same value of $K_{\min}$ is obtained from Eq. (3.5) by averaging over the angle θ. In numerical calculations, we have verified that small values of K contribute very little to the energy, so that the precise choice of $K_{\min}$ is not critical.

To obtain the energy from Eq. (2.47) we need formulas for the matrix elements

$$\mathfrak{M}^{\mathrm{dir}} = (k_0, K_0, S_0, T_0|F_0^\dagger F|T_0, S_0, K_0, k_0), \tag{3.8}$$

$$\mathfrak{M}^{\mathrm{ex}} = (k_0, K_0, S_0, T_0|F_0^\dagger FX|T_0, S_0, K_0, k_0), \tag{3.9}$$

$$\mathfrak{M} = \mathfrak{M}^{\mathrm{dir}} + \mathfrak{M}^{\mathrm{ex}}. \tag{3.10}$$

In our approximation, $\mathfrak{M}^{\mathrm{dir}}$ is

$$\mathfrak{M}^{\mathrm{dir}} = \sum_{\beta S T} \int dK\, F_0(\beta, K, S, T)F(\beta, K, S, T). \tag{3.11}$$

To evaluate $\mathfrak{M}^{\mathrm{ex}}$ we note that $F_0^\dagger F$ and X are both real and symmetric. It follows that $\mathfrak{M}^{\mathrm{ex}}$ is real as it

should be and

$$\mathfrak{M}^{ex} = (k_0, K_0, S_0, T_0 | F_0^\dagger F X | T_0, S_0, K_0, k_0)$$
$$= (k_0, K_0, S_0, T_0 | X F_0^\dagger F | T_0, S_0, K_0, k_0) . \quad (3.12)$$

This last matrix element can be written

$$\mathfrak{M}^{ex} = \frac{1}{2} \sum_{S_0' T_0'} \int dk_0' dK_0' (k_0, K_0, S_0, T_0 | X | T_0', S_0', K_0', k_0') (k_0', K_0', S_0', T_0' | F_0^\dagger F | T_0, S_0, K_0, k_0) . \quad (3.13)$$

Now we use (2.48) for X, integrate over k_0' by using the δ function, and use Eq. (2.41) to get

$$\mathfrak{M}^{ex} = \sum_{\beta S T} \int dK \, F_0^{ex}(\beta, K, S, T) F(\beta, K, S, T) , \quad (3.14)$$

where

$$F_0^{ex}(\beta, K, S, T) = \sum_{S_0' T_0'} (S_0, T_0 | \mathcal{R}(\mathcal{S}, \mathcal{T}) | T_0', S_0') \int_{|k_0 - \frac{1}{2}K_0|}^{k_0 + \frac{1}{2}K_0} (dK_0'/k_0') (k_0, K_0 | f(L) | K_0', k_0') F_0'(\beta, K, S, T) , \quad (3.15)$$

and F_0' is calculated with initial state $|k_0', K_0', S_0', T_0'\rangle$ instead of $|k_0, K_0, S_0, T_0\rangle$.

We can now outline the procedure followed in numerical calculations. The inhomogeneous term and kernel are constructed by use of Eqs. (3.1) and (3.2). Gaussian integration is used to approximate the integral equation (3.4) by a finite system of linear equations. These are solved, and the solution F is used in Eqs. (3.11) and (3.14) to find $\mathfrak{M}^{dir}$ and $\mathfrak{M}^{ex}$. These matrix elements are finally put into Eq. (2.47) to obtain the energy.

B. Finite-Rank Approximation to G_a

In general, a separate finite-rank approximation to G_a must be obtained for each allowed partial wave (lST). However, in the present work we take $l=0$ and use the Reid $^1S_0$ potential in both singlet and triplet states; so the indices lST are suppressed. With our normalization, the matrix elements of the potential V are

$$(k | V | k') = (4kk'/\pi) \int dr \, r^2 j_0(kr) V(r) j_0(k'r) , \quad (3.16)$$

and the matrix elements of G are normalized correspondingly.

The reaction matrix (2.9) depends on P (through the Pauli operator Q) and on the parameter γ^2 defined by $e_3 = k^2 + \gamma^2$. For G_a, we find from Eq. (2.33) that

$$\gamma^2 = \tfrac{1}{6}\mathcal{K}_0^2 + \tfrac{3}{4}K^2 - \omega . \quad (3.17)$$

Thus for each pair (γ^2, P) we must obtain a finite-rank approximation to $(k | G(\gamma^2, P) | k')$.

This two-parameter family of matrices is reduced to a one-parameter family by the following approximation. We combine Eq. (2.43) with Eq. (3.17) to obtain

$$P^2 = \tfrac{4}{3}\gamma^2 + \tfrac{2}{9}\mathcal{K}_0^2 + \tfrac{4}{3}\omega . \quad (3.18)$$

Now, $\frac{4}{3}\gamma^2$ varies over a range of 60 fm^{-2} or more, while the other terms on the right of Eq. (3.18) are always small and typically add up to -3.5 fm^{-2}. Therefore, we retain the correct dependence of P on γ^2, but we replace $\mathcal{K}_0$ and ω in Eq. (3.18) by fixed average values. Thus P and hence G_a become functions of γ^2 alone. Since G_a is quite insensitive to P, this should be an excellent approximation. Of course, G_a *is* sensitive to γ^2, and the dependence of G_a on γ^2 is retained without approximation. For a given value of γ^2 we construct the finite-rank approximation to G_a by choosing

$$\lambda_{ij} = w(k_i)(k_i | G | k_j) w(k_j) \quad (3.19)$$

with

$$w(k) = w_0/e . \quad (3.20)$$

We use cubic splines for the interpolating functions $s_i(k)$. The N mesh points k_i go from 0 to 5 fm^{-1} in steps of 0.25 fm^{-1} and from 5 to 12 fm^{-1} in steps of 0.5 fm^{-1}. The constant w_0 is fixed by the arbitrary convention

$$(N-1)^{-1} \sum_i |g_\beta(k_i)|^2 = \tfrac{1}{2} . \quad (3.21)$$

The most important β's are those with the largest value of $|\lambda_\beta|$. We write $1R$, $2R$, ... to indicate the β's with positive λ_β in order of decreasing magnitude $|\lambda_\beta|$, and similarly $1A$, $2A$, ... for negative λ_β.

Figure 2 is a set of plots of λ vs γ^2 for the first five β's. All λ's except for $\beta = 1R$ become nearly constant for large values of γ^2. In Fig. 3, the first five form factors g are plotted against k for

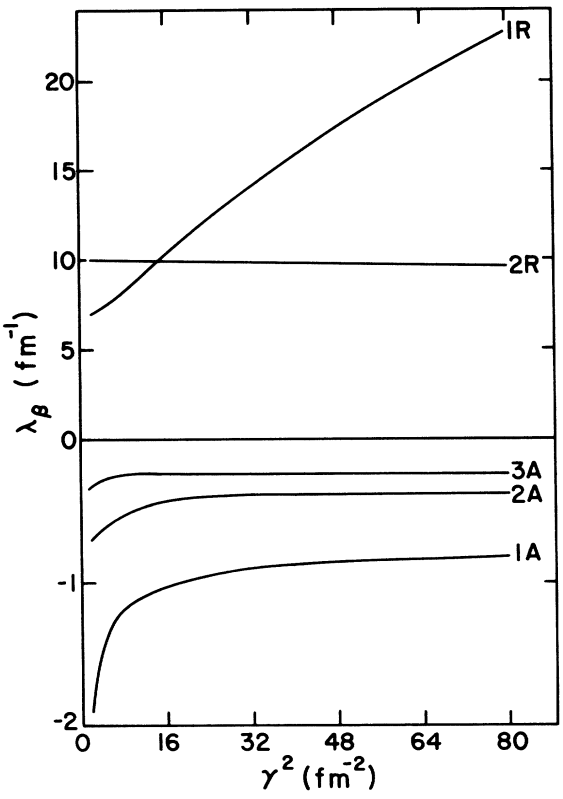

FIG. 2. The quantity λ_β plotted against γ^2 for $\beta = 1R$, $2R$, $1A$, $2A$, and $3A$. Note the different vertical scales used for positive and negative values of λ. The Reid $^1S_0$ Yukawa core potential was used, with $k_F = 1.36$ fm^{-1}.

$\gamma^2 = 14$ fm^{-2}, a typical value. The form factors with smaller $|\lambda|$ tend to have more rapid oscillations. The $2R$ form factor behaves differently from the others, remaining very small for $k < 5$ fm^{-1}.

The $1A$ form factor is plotted against k for five different values of γ^2 in Fig. 4. The form factor varies smoothly with γ^2, the most rapid variation coming at small values of γ^2. The dependence of the other form factors on γ^2 is very similar.

How accurately is $(k'|G_a|k)$ represented by the separable approximation

$$(k'|G_a|k) \approx (k'|G_a^{(n)}|k) \equiv \sum_{\beta \le n} g_\beta(k')\lambda_\beta g_\beta(k) \quad (3.22)$$

for various ranks n? As a measure of the error, we compute the quantities

$$\Delta(k_0) = \frac{\int_0^{k_0} dk \int_0^{k_0} dk' \left|(k'|G_a|k) - (k'|G_a^{(n)}|k)\right|}{\int_0^{k_0} dk \int_0^{k_0} dk' \left|(k'|G_a|k)\right|} \quad (3.23)$$

for $k_0 = 2$, 4, 6, 8, and 10 fm^{-1}. Table I shows these average errors for $\gamma^2 = 14$ fm^{-2}. The results are similar for other values of γ^2.

The $1R$ form factor by itself is seen to be good to 10–15%, except for small k, k' below 2 fm^{-1}. Adding the $1A$ and $2A$ form factors results in substantial improvement. The $2R$ form factor affects only the region of large momenta, as is expected on the basis of Fig. 3.

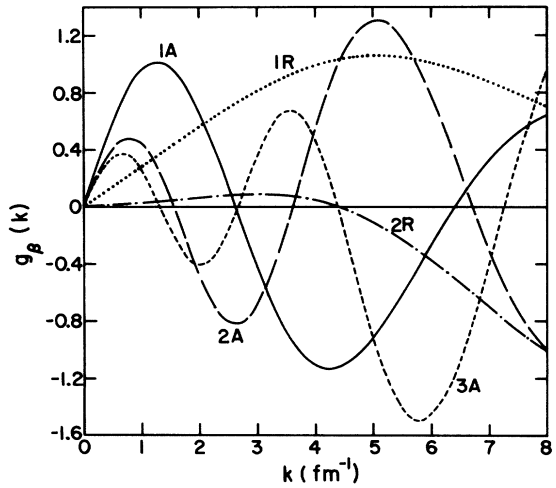

FIG. 3. The k dependence of the dimensionless form factors $g_\beta(k)$, used in the approximation (3.22) to G_a, for $\beta = 1R$, $2R$, $1A$, $2A$, and $3A$. The Reid $^1S_0$ Yukawa core potential was used, with $\gamma^2 = 14$ fm^{-2} and $k_F = 1.36$ fm^{-1}.

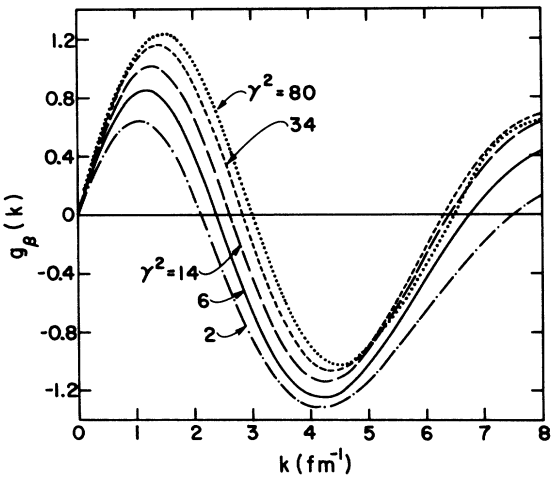

FIG. 4. Plot of the dimensionless form factor $g_\beta(k)$ vs k for $\beta = 1A$ and five different values of γ^2. The value of γ^2 for each curve is shown in the figure (in units of fm^{-2}). The Reid $^1S_0$ Yukawa core potential was used, with $k_F = 1.36$ fm^{-1}.

In numerical work, we must interpolate the g_β in both k and γ^2. The interpolation in k was done on the 35-point mesh by use of a cubic-spline formula and produced an error much less than 0.01 MeV in $\mathcal{E}_3$. After interpolation in k, we interpolated in γ^2 by use of the 5-point mesh $\gamma^2 = 2, 6, 14, 34, 80$ fm^{-2}. Within the first and last intervals, quadratic interpolation was used. In interior intervals a cubic formula was used.

For the repulsive λ's we interpolated in γ^2 in the same way. As seen in Fig. 2, attractive λ's vary rapidly for small γ^2 in a manner well represented by an inverse power of γ^2. We therefore approximate the function $\bar{\lambda}(\gamma^2) = a[\lambda(\gamma^2) + b]^{-1}$ by cubic interpolation functions. The constants a and b are determined by the requirements $\bar{\lambda}(\gamma^2) = \gamma^2$ at $\gamma^2 = 2$ and 80 fm^{-2}.

Interpolation of the g's and λ's as functions of γ^2 produced errors in G that were smaller than the error in our rank-five approximation to G. These interpolation errors should therefore be of no importance.

Interpolating in γ^2 was found to roughly triple the computing time. It is therefore important to avoid this interpolation if possible. One possibility is to simply compute the form factor for each value of γ^2 that occurs in the three-body equations. We will find later that six or eight discrete values of K are sufficient for an accurate solution of Eq. (3.4); hence the form factors need to be computed for only six or eight values of γ^2.

More work is clearly needed to find the separable representation that is best suited to the present type of calculation. But it is encouraging that a first attempt results in the rather good accuracy shown in Table I. For example, we will find that a rank-two calculation of $\mathcal{E}_3$ is accurate to about 0.1 MeV.

TABLE I. Average relative error $\Delta(k_0)$, defined by Eq. (3.23), for various finite-rank approximations to G_a. The value of γ^2 is 14 fm^{-2} and n is the rank of the approximation. The row labeled 1R is the rank-one approximation obtained with the 1R form factor. The next row is the rank-two approximation using the 1R and 1A form factors, and so on.

		k_0 (fm^{-1})				
	n	2	4	6	8	10
1R	1	1.26	0.16	0.11	0.17	0.37
1A	2	0.14	0.029	0.034	0.13	0.33
2A	3	0.055	0.013	0.015	0.11	0.33
2R	4	0.055	0.010	0.016	0.017	0.027
3A	5	0.024	0.004	0.005	0.008	0.015

C. Test Calculations

One of our main aims is to get some idea of the feasibility of solving the full three-body problem (i.e., the problem with a realistic two-body force) in momentum space. Using Gaussian integration, we reduce the integral equation (3.4) to a system of linear equations. The most important limiting factor in solving the full problem is the size of this system of linear equations. The number of equations is $N(\beta)N(K)N(\text{discr.})$, where $N(\beta)$ is the number of terms retained in the separable approximation to G_a, $N(K)$ is the number of Gaussian points, and $N(\text{discr.})$ is the number of combinations of nonconserved discrete quantum numbers. In the present work, $N(\text{discr.}) = 2$ because the only permitted values of (S, T) are $(0, 1)$ and $(1, 0)$. In the general case, however, fewer quantum numbers are conserved, and $N(\text{discr.})$ may be 20 or more. The present work was undertaken in the hope of learning what accuracy can be attained with various values of $N(\beta)$ and $N(K)$. Then we can estimate the number of linear equations needed for the full problem.

Most of our calculations are done with fixed $\mathfrak{K}_0$ and ω. We put $\mathfrak{K}_0$ equal to its rms value $(1.8)^{1/2}k_F$, which is 1.825 fm^{-1} at $k_F = 1.36$ fm^{-1}. The value of $K_{\min} = (k_F^2 - \frac{1}{9}\mathfrak{K}_0^2)^{1/2}$ is then 1.216 fm^{-1}. We took $\omega = -3.4$ fm^{-2}, corresponding to an average single-particle energy of -47 MeV for occupied states. In order to save computing time in the test runs, we avoided interpolation of the form factors in γ^2 by evaluating them at $\gamma^2 = 14$ fm^{-2}, a reasonable average value. Similarly, we used the fixed value $\gamma_2^2 = 3$ fm^{-2} in evaluating $(k|(Q/e_2)G|k_0)$, which occurs in formula (3.1) for F_0. The values used for many of the parameters are listed in Table II.

The inhomogeneous term F_0 in Eq. (3.1) depends on K_0, k_0, S_0, T_0, $\mathfrak{K}_0$, and ω but the kernel (3.2) is independent of K_0, k_0, S_0, T_0. The numerical solution of several systems of linear equations having different inhomogeneous terms but the *same* kernel is practically as fast as the solution of a single set of linear equations. Thus it is easy to study

TABLE II. Values of parameters used in the test runs in Sec. III C.

k_F	1.36 fm^{-1}
$\mathfrak{K}_0$	1.825 fm^{-1}
ω	-3.4 fm^{-2}
$K_{\min}$	1.216 fm^{-1}
γ_2^2	3 fm^{-2}
γ_3^2	14 fm^{-2}
$N(k') = N(K_0')$	6 or 10
$N(K_0)$	5
$N(k_0)$	1

TABLE III. Values of $\langle (K_0/k_F)^m (k_0/k_F)^n \rangle$, averaged over the Fermi sea according to Eq. (3.24).

m \ n	0	1	2	3	4	5
0	1.000 00	0.514 29	0.300 00	0.190 48	0.128 57	0.090 91
1	0.595 71	0.299 88	0.172 06	0.107 81	0.071 99	0.050 44
2	0.400 00	0.196 40	0.110 48	0.068 11	0.044 87	0.031 08
3	0.292 63	0.139 89	0.076 99	0.046 62	0.030 24	0.020 67
4	0.228 57	0.106 30	0.057 19	0.033 96	0.021 67	0.014 60
5	0.188 09	0.085 10	0.044 73	0.026 04	0.016 33	0.010 84

how the matrix elements $\mathfrak{M}$, defined by Eq. (3.10), depend upon K_0 and k_0. Neglecting the dependence on $\mathfrak{K}_0$ and ω, we evaluate $\mathfrak{M}/K_0^2 k_0^2$ for $N(K_0)$ values of K_0 and $N(k_0)$ values of k_0. These values of $\mathfrak{M}/K_0^2 k_0^2$ are fitted by a polynomial in K_0 and k_0, and $\mathfrak{M}/K_0^2 k_0^2$ is then averaged over the Fermi sea by using Table III, which can be obtained either analytically or numerically. The average given in Table III is defined for any function f by

$$\langle f \rangle = (\tfrac{4}{3}\pi k_F^3)^{-3} \int_{|\vec{p}_i| < k_F} d^3p_1 d^3p_2 d^3p_3 f(\vec{p}_1, \vec{p}_2, \vec{p}_3) . \tag{3.24}$$

In evaluating Eqs. (3.1) and (3.2) for F_0 and the kernel, the variable of integration was taken to be the variable z defined by Eq. (2.50). In Eq. (3.15) for F_0^{ex}, the variable $y = (K_0'^2 - k_0^2 - \frac{1}{4}K_0^2)/k_0 K_0$ was used. All three integrals were evaluated with the same number of Gaussian points $N(k') = N(K_0')$. In many cases ten points were used, but we found that using six points produced an error of less than 0.001 MeV in $\mathcal{E}_3$. The factor $\overline{Q}(K, k')$ in Eqs. (3.1) and (3.2) sometimes has a discontinuous derivative inside the region of integration. The high accuracy mentioned above was achieved without making special provision for this discontinuity in derivative.

By evaluating Eq. (3.1) by numerical integration, we obtained F_0 for $N(K_0)$ values of K_0 and $N(k_0)$ values of k_0. Then for each set of values of (β, K, S, T), these values of F_0 were fitted by a polynomial in K_0 and k_0. Interpolation by means of this polynomial was then used to obtain $F_0(\beta, K, S, T)$ at the points (k_0', K_0') required in the numerical evaluation of formula (3.15) for F_0^{ex}. In this way the number of times that F_0 had to be evaluated from Eq. (3.1) by numerical integration was greatly reduced.

The values of the conserved quantities $L, \mathcal{S}, \mathcal{T}$ included in the calculations are shown in Table IV, which contains our final results at three different densities. These results will be more fully discussed later. Here we simply note that contributions from $L \geq 3$ may be expected to give about

TABLE IV. Contributions of various combinations of the conserved quantum numbers L, $\mathcal{S}$, and $\mathcal{T}$ to the three-body energy $\mathcal{E}_3$ at three values of k_F. Also shown are the contributions to the lowest-order approximation $\mathcal{E}_3(3G)$. This is the result obtained by putting the kernel B equal to zero; so it is just the contribution from diagrams of third order in G. Energies are in MeV.

			$k_F = 1.10$ fm^{-1}		$k_F = 1.36$ fm^{-1}		$k_F = 1.62$ fm^{-1}	
L	$\mathcal{S}$	$\mathcal{T}$	$\mathcal{E}_3$	$\mathcal{E}_3(3G)$	$\mathcal{E}_3$	$\mathcal{E}_3(3G)$	$\mathcal{E}_3$	$\mathcal{E}_3(3G)$
0	$\frac{1}{2}$	$\frac{1}{2}$	0.045	0.393	0.379	1.553	1.433	4.633
0	$\frac{1}{2}$	$\frac{3}{2}$	−0.001	0.000	−0.002	−0.002	−0.011	−0.011
0	$\frac{3}{2}$	$\frac{1}{2}$	−0.001	0.000	−0.002	−0.002	−0.011	−0.011
1	$\frac{1}{2}$	$\frac{1}{2}$	−0.012	−0.012	−0.034	−0.032	−0.094	−0.088
1	$\frac{1}{2}$	$\frac{3}{2}$	−0.023	−0.022	−0.062	−0.058	−0.165	−0.152
1	$\frac{3}{2}$	$\frac{1}{2}$	−0.023	−0.022	−0.062	−0.058	−0.165	−0.152
2	$\frac{1}{2}$	$\frac{1}{2}$	−0.006	−0.006	−0.021	−0.021	−0.075	−0.074
2	$\frac{1}{2}$	$\frac{3}{2}$	−0.001	−0.001	−0.005	−0.005	−0.017	−0.017
2	$\frac{3}{2}$	$\frac{1}{2}$	−0.001	−0.001	−0.005	−0.005	−0.017	−0.017
Total			−0.023	0.329	0.185	1.370	0.879	4.111

TABLE V. Values of $\mathcal{E}_3$ for different finite-rank approximations to G_a. All other parameters are held fixed.

Approximation to G_a	$\mathcal{E}_3$ (MeV)	Change in $\mathcal{E}_3$ relative to $1R+1A$ calculation (MeV)
$1R+1A$	0.320	
$1R$	1.465	+1.145
$1R+1A+2A$	0.243	−0.077
$1R+1A+2R$	0.335	+0.015
$1R+1A+3A$	0.302	−0.018

TABLE VII. Effect of varying $N(K)$.

$N(K)$	$\mathcal{E}_3^{\rm dir}$ ($L=0$, $S=T=\frac{1}{2}$) (MeV)	$\mathcal{E}_3$ (MeV)
14	0.4673	0.2399
12	0.4674	0.2401
10	0.4666	0.2405
8	0.4689	0.2392
6	0.4625	0.2448
4	0.5284	0.3010

0.01 MeV at $k_F = 1.36$ fm^{-1} and several times this at $k_F = 1.62$ fm^{-1}. Also, since either S or T must be equal to zero, states with $S=T=\frac{3}{2}$ do not occur.

In order to determine reasonable values for $N(\beta)$, $K_{\max}$, and $N(K)$, we vary each of these parameters in turn, keeping all other parameters fixed at the values shown in Table II. As mentioned earlier, the cutoff $k_{\max}$ is always put equal to $K_{\max}$.

Taking $k_{\max} = K_{\max} = 12$ fm^{-1} and $N(K) = 14$, we calculated $\mathcal{E}_3$ for various finite-rank approximations to G_a. The results are shown in Table V. (The $1R$ calculation was actually done with $k_{\max} = K_{\max} = 8$ fm^{-1}, which will be seen shortly to give practically the same result as $k_{\max} = K_{\max} = 12$ fm^{-1}.) The $1R$ approximation is seen to be completely inadequate, but the $1R+1A$ calculation is very accurate. The $2A$ form factor contributes a little less than 0.1 MeV of attraction, and the $2R$ and $3A$ form factors give practically nothing. Thus a rank-two calculation should be accurate to about 0.1 MeV, and including the $2A$ form factor reduces this error to a small fraction of 0.1 MeV. The $1R+1A+2A$ representation of G_a is clearly adequate for all practical purposes, and we use it from now on.

Next, using the $1R+1A+2A$ representation of G_a, we vary $K_{\max}$ for fixed $N(K) = 14$. The results are shown in Table VI. Both $\mathcal{E}_3$ and the largest single contribution $\mathcal{E}_3^{\rm dir}$, which comes from the direct term with $L=0$ and $S=T=\frac{1}{2}$, are shown. The cutoff value $K_{\max} = 8$ fm^{-1} produces an error of about 0.01 MeV in the direct $L=0$ contribution. The error rises rapidly as $K_{\max}$ is reduced below 8 fm^{-1}. Thus we take $K_{\max} = 8$ fm^{-1} as a reasonable value for further calculations. Cancellation of errors makes $\mathcal{E}_3$ more accurate than the direct $L=0$ contribution, but this cancellation may be fortuitous.

TABLE VI. Effect of varying $K_{\max} = k_{\max}$.

$k_{\max} = K_{\max}$ (fm^{-1})	$\mathcal{E}_3^{\rm dir}$ ($L=0$, $S=T=\frac{1}{2}$) (MeV)	$\mathcal{E}_3$ (MeV)
12	0.480	0.243
10	0.479	0.243
9	0.476	0.241
8	0.467	0.240
7	0.448	0.240
6	0.538	0.259
5	0.350	0.312

Using $K_{\max} = 8$ fm^{-1} along with the $1R+1A+2A$ representation of G_a, we varied $N(K)$ and obtained the results shown in Table VII. Even with only six values of K, the error is less than 0.01 MeV. However, in all further calculations we have used $N(K) = 8$.

Another numerical test was to vary the value of $K_{\min}$. So far, we have somewhat arbitrarily used $K_{\min} = (k_F^2 - \frac{1}{9}\mathcal{K}_0^2)^{1/2}$, expecting that smaller values of K will contribute negligibly. If this is indeed true, the energy should be insensitive to reasonable variations in $K_{\min}$. Table VIII shows the results for three different values of $K_{\min}$. The results indicate that all reasonable values of $K_{\min}$ in the neighborhood of k_F give the same energy to within about 0.01 MeV. The insensitivity of $\mathcal{E}_3$ to $K_{\min}$ means that small values of K are unimportant. This fact suggests that the angle-average treatment of Q will cause little error. However, the situation will be less good for the tensor force, which strongly excites particles into the region just above the Fermi surface.

How many points $N(K_0)$, $N(k_0)$ are needed in order to obtain an accurate value of $\mathfrak{M}/K_0^2 k_0^2$ averaged over the Fermi sea? Table IX gives some information on this. The accurate result obtained with just one point in the Fermi sea is somewhat fortuitous. For example, the value of $\mathfrak{M}^{\rm dir}/K_0^2 k_0^2$, with

TABLE VIII. Effect of varying $K_{\min}$.

$K_{\min}$ (fm^{-1})	$\mathcal{E}_3^{\rm dir}$ ($L=0$, $S=T=\frac{1}{2}$) (MeV)	$\mathcal{E}_3$ (MeV)
1.216	0.469	0.239
1.4	0.465	0.235
1.6	0.460	0.228

TABLE IX. Dependence of calculated energy on $N(K_0)$ and $N(k_0)$.

$N(K_0)$	$N(k_0)$	$\mathcal{E}_3^{\rm dir}$ ($L=0$, $\mathcal{S}=\mathcal{T}=\frac{1}{2}$) (MeV)	$\mathcal{E}_3$ (MeV)
1	1	0.488	0.255
4	2	0.461	0.241
4	3	0.465	0.240
4	4	0.465	0.240
3	3	0.467	0.239
4	3	0.465	0.240
5	3	0.465	0.240

$L=0$, $\mathcal{S}=\mathcal{T}=\frac{1}{2}$, can change by nearly a factor 2 as K_0 and k_0 vary. In the further calculations described in subsection D, we have taken $N(K_0)=4$, $N(k_0)=3$.

Let us summarize the main results of this subsection. A rank-two calculation is accurate to about 0.1 MeV, and a rank-three calculation is accurate to about 0.02 MeV. Contributions from $L\geq 3$ are only about 0.01 MeV at $k_F=1.36$ fm^{-1} and are several times larger at $k_F=1.62$ fm^{-1}. All momentum integrations can safely be cut off at 8 fm^{-1}. Using six Gaussian points in K gives an accuracy of about 0.01 MeV. Small values of K are unimportant, so that reasonable changes in $K_{\rm min}$ produce little change in the energy. A small number of values of K_0, k_0 gives a highly accurate average of $\mathfrak{M}/K_0^2 k_0^2$ over the Fermi sea.

D. Numerical Results

In this subsection we present some of the results obtained from our momentum-space calculations. We use a pure S-wave two-body force, consisting of the Reid $^1S_0$ potential acting in both singlet and triplet states. In all calculations in this subsection, interpolation in γ^2 has been properly carried out for the form factors and for $(k|e^{-1}G|k_0)$. The parameters used in many of the calculations are shown in Table X. Calculations

TABLE X. Values of parameters used in the numerical calculations in Sec. III D.

k_F	1.36 fm^{-1}
$\mathfrak{K}_0$	1.825 fm^{-1}
ω	−3.4 fm^{-2}
$K_{\rm min}$	1.216 fm^{-1}
$N(k')=N(K'_0)$	6
$N(K_0)$	4
$N(k_0)$	3
$N(K)$	8
$K_{\rm max}=k_{\rm max}$	8 fm^{-1}
$N(\beta)$	$3(1R+1A+2A)$

TABLE XI. Contributions of various β to the dimensionless quantity $\mathfrak{M}=\mathfrak{M}^{\rm dir}+\mathfrak{M}^{\rm ex}$ given by Eqs. (3.11) and (3.14). Initial momenta were $K_0=0.598$ fm^{-1} and $k_0=0.680$ fm^{-1}. The conserved quantum numbers are $L=0$, $\mathcal{S}=\mathcal{T}=\frac{1}{2}$. All other parameters are given in Table X. Each entry is to be multiplied by 10^{-3}.

β	Exact result	Lowest order
$1R$	6.46	12.76
$1A$	−4.66	−4.09
$2A$	−0.20	−0.19
Total	1.60	8.48

in which k_F, $\mathfrak{K}_0$, ω, and $K_{\rm min}$ are varied will also be discussed.

Let us first look at the behavior of the functions F_0 and F for $\mathcal{S}=\mathcal{T}=\frac{1}{2}$. Since $(S,T)=(0,1)$ or $(1,0)$, we specify the spin-isospin argument of F_0 or F simply by giving the value of S. Also, we plot curves only for initial spin $S_0=0$; since we use spin-independent forces, the curves with $S_0=1$ give nothing new. Then from Eqs. (3.1) and (2.52) it follows that the spin-isospin coupling gives

$$F_0(\beta,K,S=1)=-3F_0(\beta,K,S=0)\,. \tag{3.25}$$

In Figs. 5–7 the functions $F_0(S=0)$, $\lambda^{-1}F(S=0)$, and $-(3\lambda)^{-1}F(S=1)$ are plotted against K for $L=0$ and three values of β. Similar plots for $L=1$ are shown in Figs. 8–10. The three functions plotted are equal in lowest order, i.e., when the term involving B is neglected in Eq. (3.4). The lowest-order approximation to F amounts to approximating the energy by terms of third order in G.

For $L=0$, the solutions $F(S=1)$ are practically equal to the lowest-order approximations. For $S=0$, however, $F(\beta=1R)$ is completely different from the unperturbed solution. So we find, as expected, that the lowest-order approximation is inadequate. This can also be seen from the results for the energy in Table IV. For $(L\mathcal{S}\mathcal{T})=(0\,\frac{1}{2}\,\frac{1}{2})$ and $k_F=1.36$ fm^{-1}, the calculation to third order in G gives 1.55 MeV, which is much larger than the correct result 0.38 MeV.

Contributions from individual values of β to $\mathfrak{M}=\mathfrak{M}^{\rm dir}+\mathfrak{M}^{\rm ex}$ given by Eqs. (3.11) and (3.14) are shown in Table XI. There is a great deal of can-

TABLE XII. Variation of $\mathcal{E}_3$ with k_F.

k_F (fm^{-1})	ω (fm^{-2})	$\mathcal{E}_3$ (MeV)
1.10	−2.35	−0.023
1.36	−3.27	0.185
1.62	−3.81	0.879

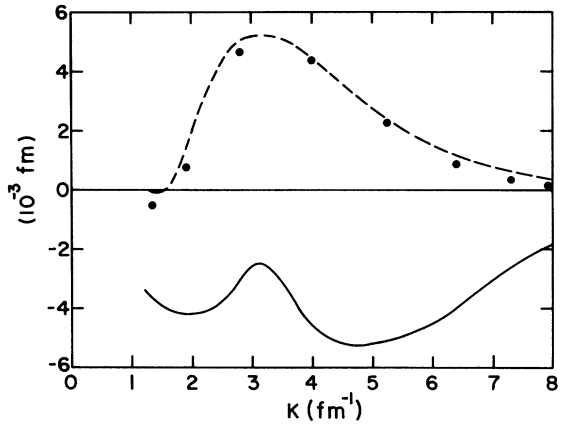

FIG. 5. Comparison between solutions $F(\beta,K,S)$ of the integral equation (3.4) and the lowest-order approximation, for $\beta=1R$. Discrete points: $F_0(\beta,K,S=0)$. Solid curve: $[\lambda_\beta(K)]^{-1}F(\beta,K,S=0)$. Dashed curve: $-[3\lambda_\beta(K)]^{-1}F(\beta,K,S=1)$. In lowest order, these three functions are equal. The initial state had $K_0=0.598$ fm^{-1}, $k_0=0.680$ fm^{-1}, $L=0$, $s=\tau=\frac{1}{2}$, $S_0=0$. The Reid $^1S_0$ Yukawa core potential was used, with $k_F=1.36$ fm^{-1}.

cellation between the attractive and repulsive components of the G matrix. The final result $\mathfrak{M}=1.60$ is only 15% of the sum of the absolute values of the individual contributions. Dahlblom[8] found similar delicate cancellation in his coordinate-space calculations using the full Reid potential.

For $L=1$, we see from Figs. 8–10 that the lowest-order approximation to F is reasonably close to the exact solution. This is reflected in Table IV, where we see that the lowest-order approximation to the energy, which is of third order in G, is very accurate for $L>0$. This is reasonable on physical grounds. The failure of the lowest-order result is known to come from

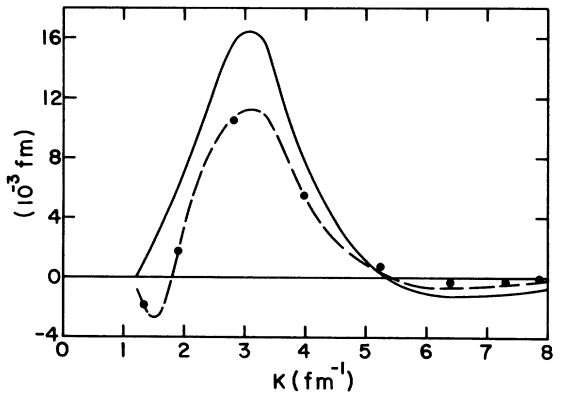

FIG. 6. Same as Fig. 5 except that $\beta=1A$.

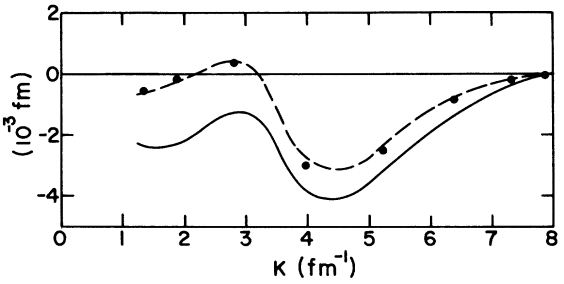

FIG. 7. Same as Fig. 5 except that $\beta=2A$.

the strong short-range correlations that occur when all three particles are close together.[3,4] For $L>0$, the centrifugal barrier prevents all three particles from coming close together at the same time, and the lowest-order result is therefore a good approximation.

We also see from Table IV that the contribution to $\mathcal{E}_3$ is very small for $L=0$ and $s=\frac{3}{2}$ or $\tau=\frac{3}{2}$. This can be understood by noting that the spatial part of the initial wave function is $j_0(K_0R)\,j_0(k_0r)$, where R and r are coordinates conjugate to K_0 and k_0, respectively. For the small values of K_0 and k_0 that occur in the Fermi sea, this expression is approximately equal to 1. Hence the spatial wave function is nearly symmetric in all three particles. A totally antisymmetric spin-isospin function is therefore required. But this is impossible for $s=\frac{3}{2}$ or $\tau=\frac{3}{2}$. Thus most of the initial-state wave function is annihilated by antisymmetrization, and only a small energy contribution survives.

The variation of $\mathcal{E}_3$ with k_F, i.e., with density,

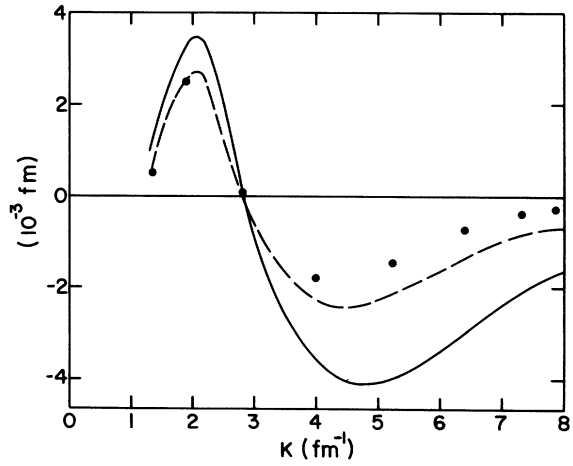

FIG. 8. Same as Fig. 5, with $\beta=1R$, except that the initial state is defined by $K_0=1.215$ fm^{-1}, $k_0=1.207$ fm^{-1}, $L=1$, $s=\tau=\frac{1}{2}$, $S_0=0$.

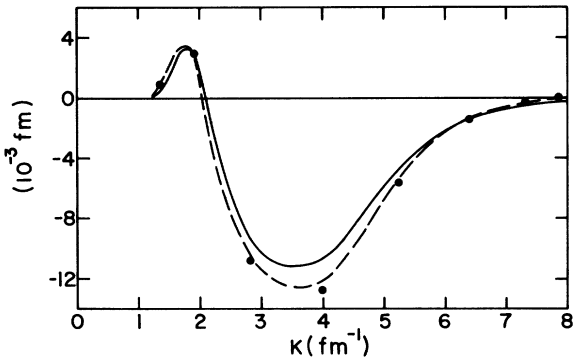

FIG. 9. Same as Fig. 8 except that $\beta = 1A$.

is shown in Table XII. In each case we took $\mathcal{K}_0^2$ equal to its mean value $1.8k_F^2$ and used Eq. (3.7) for $K_{\min}$. The values of ω are average values obtained from curves calculated by Banerjee and Sprung,[1] who used the full Reid potential in a self-consistent two-body calculation. Other parameters are the same as in Table X. The values of P required for the separable approximation to G_a were obtained from Eq. (3.18). In each case we used $\mathcal{K}_0 = (1.8)^{1/2}k_F$ and took ω from Table XII, except that the value $\omega = -3.40$ fm^{-2} was used for $k_F = 1.36$ fm^{-1}. Our calculated values of $\mathcal{E}_3$ are plotted against k_F in Fig. 11.

The density dependence of $\mathcal{E}_3$ affects both the equilibrium density and the compressibility parameter C, defined by

$$C = k_F^2(d^2\mathcal{E}/dk_F^2). \tag{3.26}$$

The expansion $\mathcal{E} = 0.3k_F^2 + \mathcal{E}_2 + \mathcal{E}_3 + \cdots$ then leads to $C = C_0 + C_2 + C_3 + \cdots$. Fitting our results for $\mathcal{E}_3$ with a quadratic in k_F, we find that at the normal

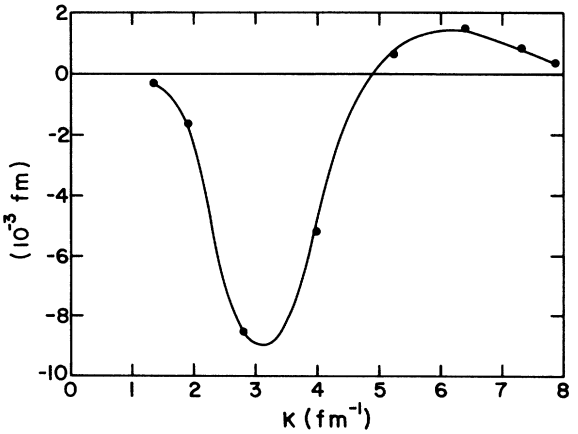

FIG. 10. Same as Fig. 8 except that $\beta = 2A$. Also, the dashed curve is not shown because it nearly coincides with the solid curve.

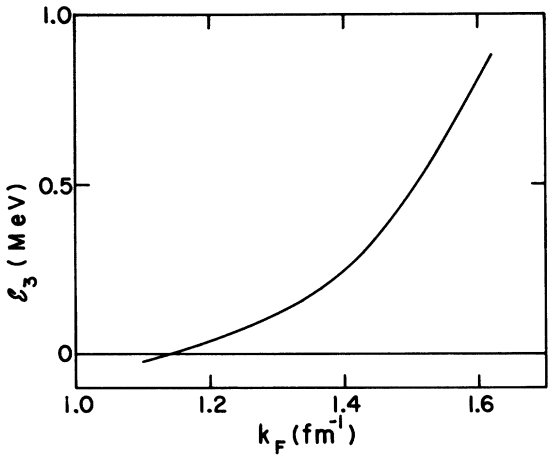

FIG. 11. Plot of the three-body energy $\mathcal{E}_3$ vs k_F. The pure S-wave two-body force is the Reid $^1S_0$ Yukawa core potential in both singlet and triplet states.

density $k_F = 1.36$ fm^{-1} the term C_3 is

$$C_3(k_F = 1.36 \text{ fm}^{-1}) = 13 \text{ MeV}. \tag{3.27}$$

Calculated values of $(C_0 + C_2)$ usually lie between 100 and 200 MeV. Banerjee and Sprung[1] obtain 140 MeV.

The effect of $\mathcal{E}_3$ on the equilibrium density can be roughly estimated as follows. If k_{F_0} is the minimum point for $(0.3k_F^2 + \mathcal{E}_2)$, then near $k_F = k_{F_0}$ we

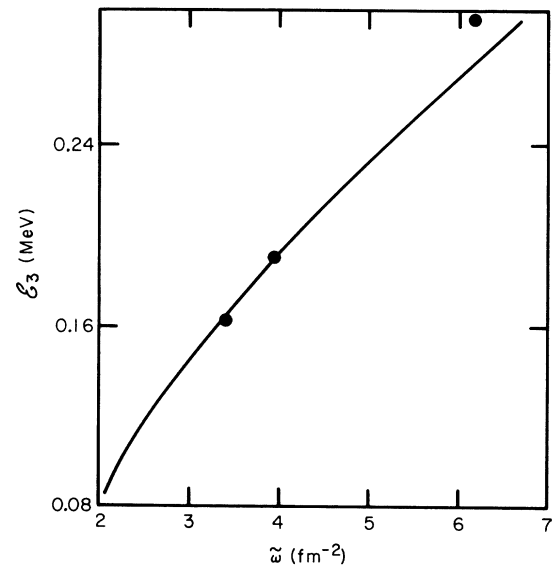

FIG. 12. Plot of the three-body energy $\mathcal{E}_3$ against the quantity $\tilde{\omega} \equiv -\omega + \frac{1}{6}\mathcal{K}_0^2$. The solid curve is obtained by varying ω for fixed $\mathcal{K}_0 = 1.825$ fm^{-1}. The three discrete points are obtained by varying $\mathcal{K}_0$ for fixed $\omega = -3.40$ fm^{-2}. All other parameters are the same as in Table X.

have

$$0.3k_F^2 + \mathcal{E}_2 \approx \text{const} + \tfrac{1}{2}(k_F - k_{F_0})^2 \times (d^2/dk_F^2)(0.3k_F^2 + \mathcal{E}_2)|_{k_{F_0}}, \quad (3.28)$$

$$\mathcal{E}_3 \approx \text{const} + (k_F - k_{F_0})(d\mathcal{E}_3/dk_F)|_{k_{F_0}}. \quad (3.29)$$

Minimizing the sum of these two expressions with respect to k_F gives

$$k_F - k_{F_0} = -(C_0 + C_2)^{-1} k_{F_0}^2 (d\mathcal{E}_3/dk_F)|_{k_{F_0}}. \quad (3.30)$$

Using our values of $\mathcal{E}_3$ and taking $k_{F_0} = 1.36$ fm^{-1} gives

$$k_F - k_{F_0} = -(3.2 \text{ MeV fm}^{-1})/(C_0 + C_2) \quad (3.31)$$

for the shift in the equilibrium value of k_F due to three-body correlations.

We see from Eqs. (3.27) and (3.31) that the present values of $\mathcal{E}_3$ change the properties of the system only slightly from those obtained in a two-body calculation. This is perfectly reasonable because the effect of $\mathcal{E}_3$ is expected to be smaller than that of $\mathcal{E}_2$ by roughly a factor κ, where κ is the healing parameter.[22] For the present two-body force, we have[23] $\kappa \approx 0.044$ at $k_F = 1.36$ fm^{-1}. For the full Reid potential, κ is more than three times as large,[23] so that $\mathcal{E}_3$ will probably have a bigger effect than we obtain here.

Since we have used average values of $\mathcal{K}_0$ and ω in all calculations so far, it is important to see how sensitive the energy is to the choice of ω and $\mathcal{K}_0$. Therefore, we have calculated the results listed in Table XIII and plotted in Fig. 12. The value $\omega = -6.15$ fm^{-2} used in Table XIII corresponds to an initial state in which all three particles have zero momentum. The value $\omega = -1.53$ fm^{-2} corresponds to an initial momentum k_F for each particle. The solid line in Fig. 12 shows that over this extreme range of ω, $\mathcal{E}_3$ varies very smoothly from 0.086 to 0.296 MeV. It would be surprising if we made an error as large as 0.05 MeV by calculating at the average value of ω.

The value of $\mathcal{K}_0$ enters the calculation in two ways. The energy denominators depend on $\mathcal{K}_0$, and so does $\bar{Q}(P, k)$ because P depends on $\mathcal{K}_0$ through Eq. (2.43). From Eqs. (2.54) and (2.56) we see that $\mathcal{K}_0$ and ω appear in the energy denominators only in the combination $-\omega + \frac{1}{6}\mathcal{K}_0^2$. Thus to test the effect of varying Q without varying the energy denominators, one should vary $\mathcal{K}_0$ while keeping $-\omega + \frac{1}{6}\mathcal{K}_0^2$ fixed.

Instead, however, $\mathcal{K}_0$ was varied for fixed ω to obtain the values $\mathcal{E}_3$ in the last three rows of Table XIII. In order to separate the effect of $\mathcal{K}_0$ on Q from its effect on the energy denominators, we have plotted $\mathcal{E}_3$ against $-\omega + \frac{1}{6}\mathcal{K}_0^2$. For fixed $\mathcal{K}_0$, this is just a plot of $\mathcal{E}_3$ against ω (solid line in Fig. 12). For fixed ω, we get a different curve (discrete points in Fig. 12). If $\mathcal{K}_0$ did not affect $\mathcal{E}_3$ by way of Q, then this curve would coincide with the solid curve – and actually the two curves lie very close together. Thus we conclude that the detailed treatment of Q is not very important, and nearly all the effect of varying $\mathcal{K}_0$ is through the energy denominators.

TABLE XIII. Values of $\mathcal{E}_3$ for the indicated values of $\mathcal{K}_0$ and ω. In each case, $K_{\min}$ was computed from Eq. (3.7). All other parameters are those of Table X.

ω (fm^{-2})	$\mathcal{K}_0$ (fm^{-1})	$-\omega + \frac{1}{6}\mathcal{K}_0^2$	$\mathcal{E}_3$ (MeV)
−1.53	1.825	2.08	0.086
−6.15	1.825	6.70	0.296
−3.40	0	3.40	0.163
−3.40	1.825	3.96	0.190
−3.40	4.08	6.17	0.296

IV. CONCLUSIONS

The main purpose of this work has been to learn whether or not a momentum-space calculation of three-body correlations in nuclear matter is feasible with the full nucleon-nucleon force. This depends mainly on the number of linear equations to be solved, which is equal to $N(\beta)N(K)N(\text{discr.})$. Here, $N(\beta)$ is the number of form factors in the finite-rank representation of G, $N(K)$ is the number of Gaussian points in the continuous variable K, and $N(\text{discr.})$ is the number of different combinations of nonconserved quantum numbers.

For the $^1S_0$ state of the Reid[12] potential, a rank-two representation of G gives an error of 0.1 MeV in $\mathcal{E}_3$, and a rank-three approximation is accurate to about 0.02 MeV. Other partial waves remain to be investigated. The tensor-coupled partial waves may be harder to fit with a low-rank approximation. On the other hand, we have fitted $(k|G|k')$ for $0 < k, k' < 12$ fm^{-1}. When the fit is restricted to $0 < k, k' < 8$ fm^{-1}, which we have found to be sufficient, a given accuracy may be attainable with a lower-rank approximation. It seems reasonable to expect adequate accuracy with a value of $N(\beta)$, averaged over partial waves, between 2 and 3.

We have seen that $N(K) = 8$ gives very high accuracy. How large is $N(\text{discr.})$ when the full two-body potential is included? A reasonable set of variables to use for the full problem is $\vec{\mathcal{K}}_0$, $\mathcal{T}$, $\mathcal{T}_z$, $\mathcal{J}, \mathcal{J}_z, K$, $(L, \frac{1}{2})J, \beta, (l, S)j, T$. Here, L is coupled to the spin of the third particle to give J, and l and S are coupled to j. Finally, J and j are coupled to $\mathcal{J}, \mathcal{J}_z$. When an angle-averaged Pauli

operator is used, $\mathcal{J}$ and $\mathcal{J}_z$ are conserved. Also conserved are $\mathcal{T}$, $\mathcal{T}_z$, and the parity $\mathcal{P} = (-1)^{L+l}$. The nonconserved discrete quantum numbers are L, J, l, S, j, and T. For $(\mathcal{J}, \mathcal{P}, \mathcal{T}) = (\frac{1}{2}, +, \frac{1}{2})$, which is the combination that Depp found to give the largest single contribution to $\mathcal{E}_3$, we find $N(\text{discr.}) = 16$ (this assumes $L \leq 2$ and $l \leq 2$). Taking $N(\beta) = 2$, we get

$$N(\beta)N(K)N(\text{discr.}) = 2 \times 8 \times 16 = 256 \qquad (4.1)$$

as the number of linear equations to be solved. If $N(\beta) = 3$, the number of linear equations increases to 384. A simple calculation by Depp[13] suggests that omitting states with $l \geq 3$ causes an error of about 2%.

Such large systems of linear equations are not beyond the power of existing computers. But their solution is a big problem, both in computing time and data management. However, the situation is probably much more favorable than this. It seems likely that accurate results can be obtained by solving the full integral equation only for the lowest values of l and L, and then including higher values of l, L by iteration, i.e., by perturbation theory. Depp[13] finds that all states, except those having the lowest allowed value of L and $l = 0$ or 1, can be treated in lowest order. And in the present calculations we have found that treating states with $L > 0$ in lowest order is an excellent approximation. This idea is also consistent with the well-established fact[3,4] that it is only the strong short-range correlations that require a full solution of the integral equation, and these correlations are most important in states with $L = l = 0$.

Thus we are optimistic about the possibility of doing accurate three-body calculations in momentum space for nuclear matter. It seems quite possible that accurate results can be obtained by solving systems of linear equations whose sizes are not much larger than 100×100. However, any such calculation will be *quite* complicated because of the many quantum numbers and the complicated angular momentum coupling that are involved.

The results that we have obtained for $\mathcal{E}_3$ as a function of k_F should be accurate for the assumed two-body force but are merely illustrative. We have used a pure S-wave force consisting of the Reid $^1S_0$ potential acting in both singlet and triplet states. The numerical results will almost certainly be very different when the complete two-body force is used. With our force we would expect *a priori* to find $\mathcal{E}_3 \approx \kappa \mathcal{E}_2$, where κ is the healing parameter. Taking[23] $\kappa \approx 0.044$ and $\mathcal{E}_2 \approx -30$ MeV gives $\mathcal{E}_3 \approx -1.3$ MeV. The fact that we actually find $\mathcal{E}_3 \approx 0.2$ MeV at normal density illustrates again the large amount of cancellation that is taking place between the attractive and repulsive parts of the force.

It would be of great interest to compare the results of the present calculation with those obtained with the coordinate-space method for the same two-body force. Unfortunately, an essential assumption of the coordinate-space method is the existence of a strong short-range repulsive force in all partial waves.[5] Thus a comparison must wait until states with $l > 0$ have been included in the momentum-space calculations.

ACKNOWLEDGMENTS

The authors are indebted to F. Serduke for many informative discussions. B. Day is grateful to Professor Aage Bohr for the extremely pleasant working conditions at the Bohr Institute, and to the Guggenheim Foundation for financial support.

---

*Work performed under the auspices of the U. S. Atomic Energy Commission.

†Permanent address.

[1]P. K. Banerjee and D. W. L. Sprung, Can. J. Phys. 49, 1899 (1971).

[2]W. D. Myers and W. J. Swiatecki, Nucl. Phys. 81, 1 (1966).

[3]R. Rajaraman, Phys. Rev. 131, 1244 (1963); R. Rajaraman and H. A. Bethe, Rev. Mod. Phys. 39, 745 (1967).

[4]H. A. Bethe, Phys. Rev. 138, B804 (1965).

[5]B. Day, Phys. Rev. 151, 826 (1966).

[6]M. W. Kirson, Nucl. Phys. A99, 353 (1967).

[7]H. A. Bethe, Phys. Rev. 158, 941 (1967).

[8]T. K. Dahlblom, Proceedings of the Abo Academy, Ser. B, Vol. 29, No. 6. Available from NORDITA, Blegdamsvej 17, Copenhagen, Denmark.

[9]S. A. Moszkowski, Phys. Rev. 140, B283 (1965).

[10]B. R. Easlea, Phys. Letters 19, 662 (1966); A. G. Petschek, Phys. Rev. 154, 934 (1967).

[11]B. S. Bhakar and R. J. McCarthy, Phys. Rev. 164, 1343 (1967).

[12]R. V. Reid, Ann. Phys. (N.Y.) 50, 411 (1968).

[13]J. G. Depp, Ph.D. thesis, Carnegie-Mellon University, 1969 (unpublished), available from University Microfilms Inc., order No. 70-17139.

[14]F. Coester, in *Lectures in Theoretical Physics: Quantum Fluids and Nuclear Matter*, edited by K. T. Mahanthappa and W. E. Brittin (Gordon and Breach, New York, 1969), Vol. XIB.

[15]See ref. 14, Eqs. (V.11), (V.12), (V.17), (V.26), and (V.27).

[16]See ref. 14, Eqs. (V.26) and (V.28). There is a trivial

misprint in Eq. (V.26). Two hole-creation operators $b^+(p_1)b^+(p_2)$ should be inserted at the end of the first line.

[17]See Ref. 14, Eq. (V.27).

[18]N. M. Hugenholtz, Physica 23, 481 (1957).

[19]E. J. Irwin, Ph.D. thesis, Cornell University, 1963 (unpublished), available from University Microfilms, Inc., order No. 64-1010; C. M. Ko and D. W. Sprung, Can. J. Phys. 47, 123 (1969).

[20]E. P. Harper, Y. E. Kim, and A. Tubis, Phys. Rev. C 2, 877 (1970).

[21]R. Balian and E. Brézin, Nuovo Cimento 61B, 403 (1969).

[22]B. H. Brandow, Phys. Rev. 152, 863 (1966).

[23]A. Kallio and B. D. Day, Nucl. Phys. A124, 177 (1969).

PHYSICAL REVIEW C VOLUME 6, NUMBER 6 DECEMBER 1972

Elastic *pd* Scattering at 316, 364, 470, and 590 MeV in the Backward Hemisphere

J. C. Alder,*†‡ W. Dollhoff,‡ C. Lunke,†‡ C. F. Perdrisat,‡ W. K. Roberts, P. Kitching,§¶ G. Moss,§¶ W. C. Olsen,§¶ and J. R. Priest‖

National Aeronautics and Space Administration, Lewis Research Center, Cleveland, Ohio 44135

(Received 5 July 1972)

The results of an investigation of the elastic *pd* differential cross section for center-of-mass angles between 91 and 164° at energies of 316, 364, 470, and 590 MeV are presented. For center-of-mass scattering angles larger than 130°, the cross sections at any given angle are within 10% of each other for the three largest energies. The extrapolated 180° differential cross section observed in this experiment remains nearly constant from 316 to 590 MeV. This is in marked contrast to the rapid decrease in cross section with increasing energy observed by other investigators for both larger and smaller energies. Possible theoretical explanations of this behavior are mentioned.

INTRODUCTION

It has been known for some time that above 300 MeV, the backward elastic (*pd*) differential cross section was larger than one would expect on the basis of a single-nucleon-exchange mechanism. There was a renewed interest in this problem when data at 1300[1] and 1000 MeV,[2] and later 590 MeV[3] became available. A possible explanation of the anomalous backward scattering was proposed by Kerman and Kisslinger[4] in terms of an admixture of excited nucleon states in the ground state of the deuteron. It was found that if the probability for the ground state of the deuteron to be a normal nucleon and a $(\frac{5}{2}, \frac{1}{2})$ nucleon isobar with invariant mass 1688 MeV, was 2%, the results of experiments of Refs. 2 and 3 could be explained. The 1688-MeV isobar is the lowest nucleon excited state that can exist in the deuteron, unless both nucleons are excited. The different possible components of the deuteron ground state with isobars are discussed for example by Arenhövel, Danos, and Williams.[5]

Another model was proposed by Craigie and Wilkin[6] who argued that for laboratory energies around 600 MeV, triangular graphs with a neutron line and a pion line connecting the observed states should be more important than the one-neutron-exchange diagram. A neutron-pion-exchange graph is probably dominant in the process $pp \to d\pi^+$, which is known to have a resonant-like behavior with a maximum at 600 MeV. The resonant behavior in $d\pi^+$ final state is believed to be associated with the $(\frac{3}{2}, \frac{3}{2})$ 1236-MeV resonance in the nucleon-pion system, which would enhance reactions in which the nucleon and pion exchanged have an invariant mass near that of the $(\frac{3}{2}, \frac{3}{2})$ resonance. This situation occurs also in the *pd* system, Wilkin[7] calculated the (*pd*) elastic cross section near 180° with no free parameter and obtained excellent agreement with the data of Ref. 3.

In still another effort to understand (*pd*) scattering, Remler and Miller[8] have been investigating the lower-energy data in terms of single-nucleon exchange, single-scattering and multiple-scattering contributions. The data below 300 MeV are being used to determine a number of parameters to describe the third contribution. An extrapolation of these parameters to the energy region where other mechanisms may be important is expected to demonstrate the existence of new terms in the interaction.

At the inception of this experiment very little data outside of that previously mentioned existed above 300 MeV. Experimental data had been reported at 340[9] and 660 MeV[10] but included only a few data points in the backward hemisphere, each with relatively large uncertainties. The current